

Heavy Flavour Production at HERA

Karin Daum^{1,2}

UDC preprint
© 2003

¹University of Wuppertal
(Gaussstrasse 20, 42097 Wuppertal, Germany),

²permanent address: DESY
(Notkestrasse 85, 22607 Hamburg, Germany),

Measurements on open charm and beauty production in ep collisions at a centre-of-mass energy of $\sqrt{s} = 318$ GeV performed by the H1 and ZEUS experiments at HERA are presented. Final states containing charm are identified via reconstruction of D mesons while events containing muons and at least one jet were used to select beauty enriched data samples. The results cover the region of negative four-momentum transfer squared Q^2 from photoproduction ($Q^2 \approx 0$) to deep inelastic scattering at large Q^2 . The experimental results are compared with QCD predictions.

1. Introduction

The description of open heavy flavour production in ep scattering is based on perturbative QCD ($pQCD$). In leading order (LO) heavy quarks are predominantly produced by the *photon gluon fusion* (PGF) process, $\gamma g \rightarrow Q\bar{Q}$ ($Q = c, b$), where a quasi-real or virtual photon emitted by the electron¹ interacts with a gluon in the proton producing a heavy quark pair $Q\bar{Q}$, as shown in fig. 1a.

The kinematics of the ep interaction is described by three independent variables, the centre-of-mass energy \sqrt{s} (318 GeV at HERA), the four-momentum transfer squared of the photon $q^2 = -Q^2$ and either one of the scaling variables $y = (q \cdot P)/(l \cdot P)$, the inelasticity of the ep interaction, or Bjorken- x $x = Q^2/(2q \cdot P)$. Here P and l denote the four-momentum of the proton and the electron, respectively. The γp centre-of-mass energy squared is given by $W_{\gamma p}^2 = W^2 \approx y \cdot s - Q^2$.

The dominant contribution to heavy flavor production is due to the exchange of an almost real photon (*photoproduction*, γp), i.e. $Q^2 \approx 0$. The heavy quarks hadronize and are detected via charmed or beauty hadrons visible in the final state.

Open heavy flavor production at HERA is dominated by charm production. Due to the large mass m_b and the charge of beauty quarks the cross section for $\sigma(ep \rightarrow e b \bar{b} X)$ is expected to be roughly two orders

of magnitude smaller than $\sigma(ep \rightarrow e c \bar{c} X)$. However, the large scale m_b makes it attractive the study of beauty production in ep scattering because pQCD is expected to be more reliable than for charm production.

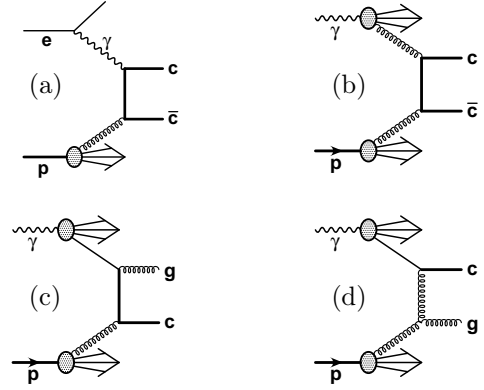


Fig.1: LO diagrams for heavy flavour photoproduction in ep collision: (a) direct (b-d) resolved contributions.

The analysis of these data starts to allow detailed testing of pQCD because of the high luminosity delivered by HERA in recent years.

2. Open Heavy Flavor Production

In LO pQCD open heavy flavor production the *direct* process ($\gamma g \rightarrow Q\bar{Q}$) dominates. In γp sizable contributions from *resolved* photon interactions, i.e. $g^{(\gamma)} g^{(p)} \rightarrow Q\bar{Q}$ (fig. 1b) and $Q^{(\gamma)} g^{(p)} \rightarrow Qg$ (figs. 1c and 1d), are expected due to the partonic structure of the photon. In next-to-leading order (NLO) or beyond, however, this distinction is inappropriate.

2.1 NLO Calculation in the DGLAP Scheme

NLO calculations are performed in several schemes. All approaches assume a scale to be hard enough to apply pQCD and to guarantee the validity of the factorization theorem.

¹Hereafter, a reference to electrons implies a reference to either electrons or positrons.

The *massive approach* is a fixed order calculation (in α_s) with $m_Q \neq 0$, assuming three active flavours in the proton. The densities of the three light quarks and the gluon in the proton and the photon are obtained by the DGLAP evolution. Heavy quark are produced perturbatively [1, 2] via PGF. These calculations are reliable for a renormalization scale $\mu_r^2 \approx m_Q^2$, but break down for $\mu_r^2 \gg m_Q^2$. Based on the NLO coefficient functions [3, 4] the Monte Carlo integration program HVQDIS [5] and the FMNR code [6] provides four-momenta of the outgoing partons in the DIS and the γp regime, respectively. By applying non-perturbative fragmentation, e.g. the longitudinal Peterson fragmentation [7], the calculation of visible differential inclusive heavy meson production cross sections becomes possible.

The *massless approach* [8, 9] sets $m_Q = 0$. Therefore the heavy quark is treated as an active flavour in the proton. This ansatz of *flavour excitation (FE)* gives rise to new processes like $Q^{(p)}g \rightarrow Qg$ and $Q^{(p)}q \rightarrow Qq \dots$. Within this approach the final state divergencies are absorbed into the fragmentation function. This scheme is indispensable for $p_\perp \gg m_Q$ but breaks down for $p_\perp \leq m_Q$.

In a third approach (*FONLL*) the features of both methods are combined. The *matched scheme* adjusts the number of partons n_f in the proton according to the relevant scale. It applies the FOPT with massive quarks at low scales and treats the heavy similar to massless quarks for scales much above m_Q . In deep inelastic scattering (*DIS*) it has been mainly applied for inclusive quantities such as σ_{tot} , F_2^Q [10] while in γp also differential cross sections are calculated [11].

2.2 CCFM Evolution

The measurements will also be compared with predictions based on the CCFM evolution equation [12]. This scheme may be most appropriate to describe the parton evolution at small x . In the parton cascade, gluons are emitted in an angular ordered region to account for coherence effects. Due to this ordering, the unintegrated gluon distribution in CCFM depends on the maximum allowed angle in addition to the momentum fraction x and the transverse momentum of the propagator gluon. The cross section is then calculated according to the k_t -factorization theorem by convoluting the unintegrated gluon density with the off-shell PGF matrix element with massive quarks.

Based on the solution of the CCFM equation [13] a full hadron level Monte Carlo generator CASCADE has

been developed [14] in which the generation of heavy quark events, including the initial state gluon radiation according to CCFM and Lund string fragmentation (JETSET) is possible. The fragmentation of charmed quarks to D^{*+} mesons is performed using the Peterson fragmentation function. The unintegrated gluon density [15] has been extracted from the H1 F_2 data [16].

3. Fragmentation of Charm Quarks

Experimentally heavy quark are not observed directly, but heavy flavored hadrons are measured instead. This fragmentation process is a long distance effect, which can only be described by phenomenological models. These models are implemented into theoretical cross section calculations assuming fragmentation to be independent of the production mechanism of the heavy quark. This universality can be tested by measuring the charm fragmentation properties also in ep collisions.

3.1 Fragmentation Ratios and Fractions

At HERA the inclusive production cross sections of the weakly decaying charm ground states: D^0 , D^\pm , D_s^\pm pseudo-scalar mesons and Λ_C^\pm baryons and also of the charmed vector meson $D^{*\pm}$ have been measured in the γp [17] and in the DIS regime [18]. In the subsequent discussion the small influence from the excited D mesons with non-zero orbital angular momenta is neglected.

The ratio $R_{u/d} = c\bar{u}/c\bar{d}$, measures the rate of the neutral to charged D meson production. Due to the smallness of the bare u and d quark masses compared to their dressed masses a value close to unity is expected in a simple picture of the QCD vacuum. The measurements of $R_{u/d}$ are shown in Fig.2 for γp , DIS together with e^+e^- -annihilation data. They all agree very well with this naive expectation. For the weighted average a value of $R_{u/d} = 1.011 \pm 0.047$ is obtained.

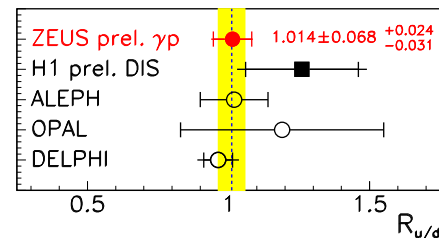


Fig.2: The ratio $R_{u/d}$ measured in ep collisions in comparison with the e^+e^- results from LEP.

Due to the higher bare s quark mass D_s^\pm mesons are expected to be less frequently produced than D^0 and D^\pm mesons. This is quantified by the

strangeness suppression factor $\gamma_s = 2 \cdot c\bar{s}/(c\bar{u} + c\bar{d})$ for which the results of γp , DIS and e^+e^- -annihilation are summarized in Fig.3. Irrespectively of the hard subprocess of charm quark production a significant strangeness suppression is observed, which averages to $\gamma_s = 0.266 \pm 0.018$. This is very consistent with the simple expectation assuming the dressed quark masses to be relevant during hadronization, which would yield an estimate of $\gamma_s = [(M_u + M_d)/(2 \cdot M_s)]^4 \approx 0.15 \dots 0.4$, where M_q denotes the dressed quark mass.

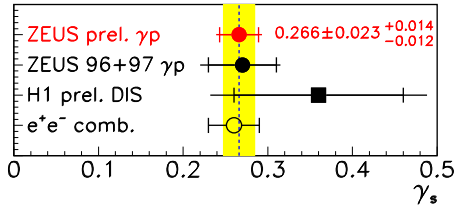


Fig.3: The strangeness suppression factor γ_s measured at HERA compared to the combined e^+e^- result.

The ratio $P_V = V/(V + P)$ of the fraction of D mesons produced in a vector state is depicted in Fig. 4. From naive spin counting a value $P_V = 3/4$ is expected while the thermodynamical approach [19] and the string fragmentation approach [20], both predict $2/3$. Independent of the production mechanism the experiments yield consistent results, which are averaged to $P_V = 0.588 \pm 0.014$ significant below the expectations.

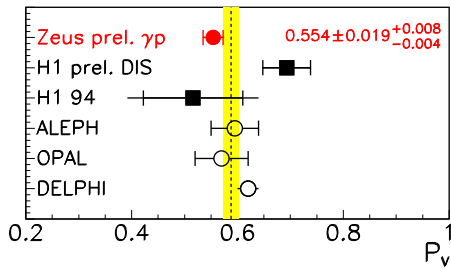


Fig.4: The fraction P_V of D meson production in the vector state measured at HERA compared to results from e^+e^- -annihilation.

Finally the cross section measurements can be converted to fractions of c quarks hadronizing as particular charmed hadrons, $f(c \rightarrow D, \Lambda_c)$. This is given by the ratio of the production cross section of a specific charmed hadron to the sum of all charmed ground state hadrons. Currently no measurement of the strange-charmed baryons Ξ_c^\pm , Ξ_c^0 and Ω_c^0 exists at HERA. Because of the strangeness suppression their contribution is expected to be small. It is estimated from the measured non-charm baryon ratios Ξ^\pm/Λ and Ω^\pm/Λ . Tab. 1 summarizes the branching fractions as

observed in γp and DIS at HERA in comparison with the combined values from e^+e^- -annihilation [21].

$f(c \rightarrow D^+)$	γp	$0.248 \pm 0.014^{+0.004}_{-0.008}$
	DIS	$0.202 \pm 0.020^{+0.045+0.029}_{-0.033-0.021}$
	e^+e^-	0.232 ± 0.010
$f(c \rightarrow D^0)$	γp	$0.557 \pm 0.019^{+0.005}_{-0.013}$
	DIS	$0.658 \pm 0.054^{+0.117+0.086}_{-0.142-0.048}$
	e^+e^-	0.549 ± 0.023
$f(c \rightarrow D_s^+)$	γp	$0.107 \pm 0.009 \pm 0.005$
	DIS	$0.156 \pm 0.043^{+0.036+0.050}_{-0.035-0.046}$
	e^+e^-	0.101 ± 0.009
$f(c \rightarrow \Lambda_c^+)$	γp	$0.076 \pm 0.020^{+0.017}_{-0.001}$
	e^+e^-	0.076 ± 0.007
$f(c \rightarrow D^{*+})$	γp	$0.233 \pm 0.009^{+0.003}_{-0.005}$
	DIS	$0.263 \pm 0.019^{+0.056+0.031}_{-0.042-0.022}$
	e^+e^-	0.235 ± 0.007

Tab.1: The fragmentation ratios $f(c \rightarrow D, \Lambda_c)$ in γp [17], DIS [18] and e^+e^- -annihilation.

The comparison of the results on the fragmentation ratios and fractions in γp and DIS at HERA and in e^+e^- -annihilation has shown that the QCD vacuum important during the hadronization of charm quarks is independent of their production mechanism.

3.2 Charm Fragmentation Function

Charm fragmentation functions are used to parameterize the energy transfer of the charm quark to a given charmed hadron. Since fragmentation is a non-perturbative process several different forms of tunable fragmentation functions have been proposed. Their parameters have been fixed from fits to data, usually from e^+e^- -annihilation experiments. Due to the limited precision of the available data the fitted fragmentation function contributes significantly to the uncertainties in calculations of inclusive D^* meson cross sections at HERA. This, in turn, limits the possible impact of the measurements of inclusive $D^{*\pm}$ production on QCD precisions tests at HERA.

In e^+e^- collisions the two initially produced charm quarks carry half of the available centre-of-mass energy, \sqrt{s} . Therefore, the fragmentation variable $z_E(D^*)$ of

a $D^{*\pm}$ meson can simply be related to the beam energy, leading to $z_E(D^*) = 2 \cdot E(D^*)/\sqrt{s}$. In ep collisions, however, the initial charm quark energy can not be determined so easily. In such an environment the charm quark energy can be approximated by the observed energy E^{jet} of the jet associated to the reconstructed $D^{*\pm}$ meson. When reconstructing jets as massless objects a possible definition of the fragmentation variable is $z(D^*) = (E + p_{\parallel})^{D^*}/(E + p_{\parallel})^{jet} \equiv (E + p_{\parallel})^{D^*}/2E^{jet}$, where p_{\parallel} denotes the longitudinal momentum of the D^* meson relative to the axis of the associated jet.

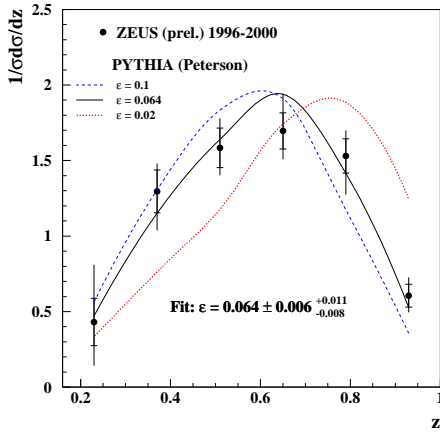


Fig.5: Relative cross section $1/\sigma(d\sigma/dz)$ for the data compared with the predictions of the PYTHIA Monte Carlo using Peterson fragmentation function with different values of ϵ .

Fig. 5 presents the normalized differential cross section, $1/\sigma(d\sigma/dz)$, in the kinematic region $Q^2 < 1 \text{ GeV}^2$ and $130 < W_{\gamma p} < 280 \text{ GeV}$ [22]. At least one jet with a transverse energy $E_T^{jet} > 9 \text{ GeV}$ and a pseudo-rapidity $|\eta^{jet}| < 2.4$ in the laboratory frame has been required to which a D^* meson with a transverse momentum $p_T^{D^*} > 2 \text{ GeV}$ and a pseudo-rapidity $|\eta^{D^*}| < 1.5$ is associated. Here, the pseudo-rapidity is defined as $\eta = -\ln \tan(\Theta/2)$. The data is compared to predictions of the Pythia Monte Carlo program using the Peterson fragmentation function [7] which has the form

$$f(z) \propto [z(1 - 1/z - \epsilon/(1 - z))^2]^{-1} \quad (1)$$

for different values of the free parameter ϵ . It can be seen that a value of $\epsilon = 0.02$ leads to a too hard while a value of $\epsilon = 0.1$ gives a too soft fragmentation. A fit of the Monte Carlo to the data yields $\epsilon = 0.064 \pm 0.006^{+0.011}_{-0.008}$.

In Fig. 6 the γp data from HERA is compared with measurements from the ARGUS [23] and the OPAL [24] collaborations in e^+e^- annihilation at two different values of s . At medium and large z the

distributions of the different processes and energies are quite similar. At low z the OPAL data show a significant contribution from the process $e^+e^- \rightarrow q\bar{q}g$ with the subsequent gluon splitting $g \rightarrow c\bar{c}$. Contributions from gluon splitting are significantly suppressed in the energy range of HERA and DORIS. Although there are differences in the definitions of the fragmentation variable for the different data this comparison suggests the charm fragmentation function to be universal in the phase regions explored by these experiments.

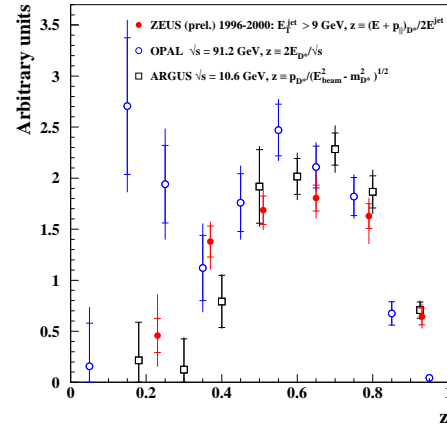


Fig.6: Fragmentation function of $D^{*\pm}$ mesons in γp at HERA (●) compared to measurements from OPAL (○) and ARGUS (□)

4. Inclusive $D^{*\pm}$ Meson Production in DIS

$D^{*\pm}$ mesons are identified by the decay chain $D^{*\pm} \rightarrow D^0\pi^\pm$, $D^0 \rightarrow K^\mp\pi^\pm$ in the visible range of the transverse momentum $p_\perp(D^*) > 1.5 \text{ GeV}$ and the pseudo-rapidity $|\eta(D^*)| < 1.5$ in the laboratory frame. For the DIS selection the event kinematics is restricted to $0.05 < y < 0.7$ and $2 \text{ GeV}^2 < Q^2 < 100 \text{ GeV}^2$ [25].

In Fig. 7 the inclusive single differential $D^{*\pm}$ cross sections in the visible region are shown as a function of the kinematic quantities Q^2 and W and as a function of the $D^{*\pm}$ observable $\eta(D^{*\pm})$. Also shown are the expectations from the NLO calculations of the HVQDIS program using the CTEQ5F3 parton density parameterization [26]. The dark shaded band indicates the uncertainties in this calculation by varying m_c and ϵ from $m_c = 1.3 \text{ GeV}$ and $\epsilon = 0.035$ (upper limit) to $m_c = 1.5 \text{ GeV}$ and $\epsilon = 0.10$ (lower limit). The fragmentation fraction $f(c \rightarrow D^{*\pm}) = 0.233 \pm 0.010 \pm 0.011$ [27] has been used. The renormalization scale and the factorization scale are set to $\mu_r^2 = \mu_f^2 = Q^2 + 4m_c^2$. Although the total visible cross section prediction of HVQDIS is smaller than experimentally observed, the agreement with the data in the shapes of the different single differential cross

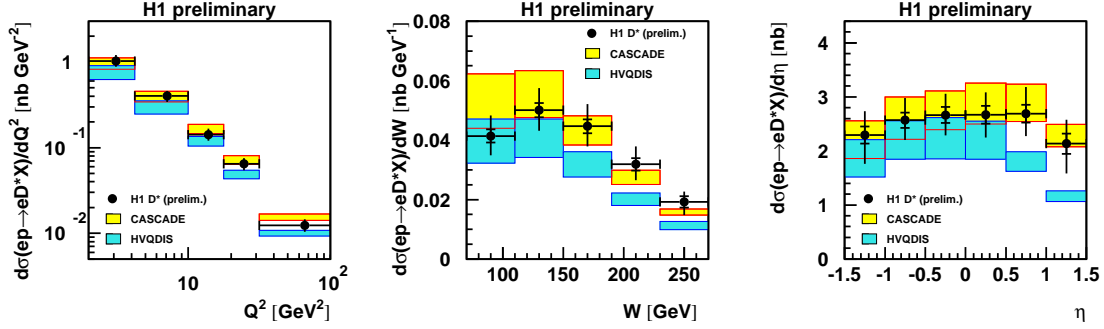


Fig. 7: Single differential inclusive cross section $\sigma(ep \rightarrow eD^{*\pm}X)$ versus Q^2 , W and η_{D^*} compared with the NLO DGLAP expectation from HVQDIS (lower shaded band) and the CCFM expectation based on the CASCADE program (upper shaded band). See text for further explanations.

sections is reasonable. A difference in shape is observed only in the $d\sigma/d\eta$ cross section. In the forward direction, the observed D^{*+} meson production cross section is considerably larger than predicted by this calculation.

Fig. 7 also includes the predictions of the CCFM calculations using the CASCADE program (light shaded band) with varying m_c between 1.3 GeV and 1.5 GeV and using $\epsilon = 0.078$. The expectations from the CASCADE program are found to agree better with data in general and especially in the forward η region, where the HVQDIS program fails to describe the data. It is interesting to note that the CCFM calculation, which starts from completely different principles and aims specifically to describe low x phenomena, is able to describe single inclusive $D^{*\pm}$ meson production at HERA better than the DGLAP based NLO calculations with the chosen settings.

is significantly above the data, at small p_t . Also shown is the prediction of the CCFM calculation using the CASCADE Monte Carlo program. As for Fig. 7 this model describes the data quite well.

In Fig. 8b the inclusive $D^{*\pm}$ meson cross section with associated di-jet production, $d\sigma(ep \rightarrow eD^{*\pm}jjX)/dE_T^{max}$, is shown. Using the k_t -cluster algorithm [29] it is required that at least 2 jets are reconstructed in the Breit frame having transverse energies of $E_T^{jet1(2)} \geq 4(3)$ GeV and pseudo-rapidities in the laboratory frame in the interval $-1 \leq \eta_{jet1,2} \leq 2.5$. While the single inclusive cross sections are well reproduced by the CASCADE program it systematically overshoots the data when studying associated di-jet production. On the other hand, the RAPGAP program, which predicts a too high single inclusive cross section, underestimates the associated di-jet production.

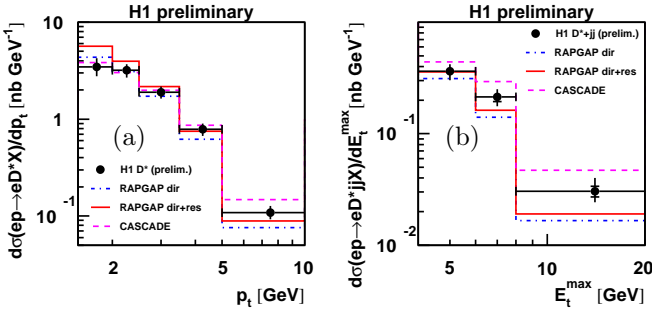


Fig.8: Cross sections (a) $d\sigma(ep \rightarrow eD^{*\pm}X)/dp_t$ and (b) $d\sigma(ep \rightarrow eD^{*\pm}jjX)/dE_t^{max}$ compared with the predictions from RAPGAP and CASCADE. See text for details.

In Fig. 8a the single inclusive cross section $d\sigma(ep \rightarrow eD^{*\pm}X)/dp_t$ is compared with the expectation of the RAPGAP Monte Carlo program [28] when only the direct process (Fig. 1a) is taken into account and when also the resolved contributions (Fig. 1b-d) are included. The RAPGAP program is based on LO DGLAP matrix element. When including all contributions the prediction

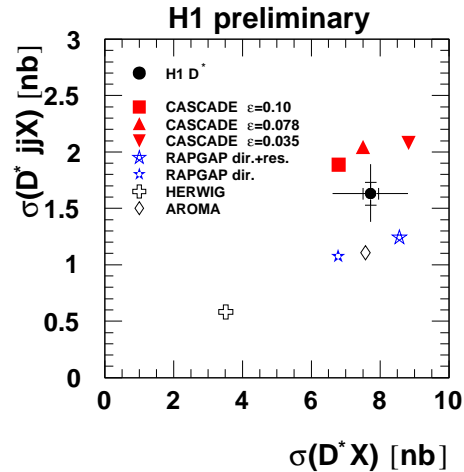


Fig.9: Measured cross sections $\sigma(ep \rightarrow eD^{*\pm}X)$ versus $\sigma(ep \rightarrow eD^{*\pm}jjX)$ compared with predictions of various Monte Carlo programs. See text for details.

The situation of inclusive $D^{*\pm}$ meson production in DIS at HERA is summarized in Fig. 9 where correlation

between the measured visible cross sections $\sigma(ep \rightarrow eD^{*\pm}X)$ and $\sigma(ep \rightarrow eD^{*\pm}jjX)$ is compared with predictions of various Monte Carlo programs considered suitable to describe heavy flavour production. The calculations with HERWIG, AROMA and RAPGAP are performed with a charm quark mass $m_c = 1.4$ GeV and the CTEQ5L proton parton densities. The resolved photon contribution in RAPGAP is computed using the GRV photon parton densities. CASCADE is based on the unintegrated gluon density obtained from a CCFM fit to the inclusive F2 data from H1 for $m_c = 1.3$ GeV, $\epsilon_c = 0.035$ for $m_c = 1.4$ GeV, $\epsilon_c = 0.078$ and for $m_c = 1.5$ GeV, $\epsilon_c = 0.10$. Within the parameter space currently explored in this analysis none of the models is able to describe simultaneously both aspects of the data.

5. Inclusive $D^{*\pm}$ Meson Production in γp

Two different ways are used to select γp events at HERA. The analysis of the ZEUS experiment [30] is based on 'no tag' events, where the outgoing electron is not detected. This requirement corresponds to a kinematic region of $Q^2 < 1$ GeV² and $130 < W_{\gamma p} < 280$ GeV. The visible range of the $D^{*\pm}$ meson is restricted to $p_t^{D^*} > 1.9$ GeV and $|\eta^{D^*}| < 1.6$. The analysis from the H1 [31] experiment is based on 'tagged' events, in which the outgoing electron is detected in the electron tagger located 33 metre down stream from the interaction point. The detection of the electron fixes the kinematic region to $Q^2 < 0.001$ GeV² and $171 < W_{\gamma p} < 256$ GeV. The visible range of the $D^{*\pm}$ meson has been limited to $p_t^{D^*} > 2.5$ GeV and $|\eta^{D^*}| < 1.5$.

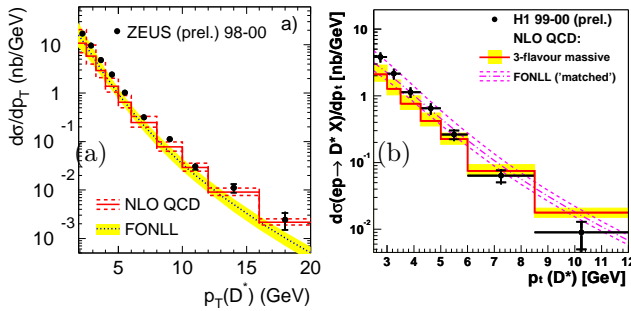


Fig.10: Cross sections $d\sigma(ep \rightarrow eD^{*\pm}X)/dp_t$ in γp in the kinematic region of (a) untagged and (b) tagged events compared with predictions from NLO QCD and FONLL.

The visible cross section $d\sigma(ep \rightarrow eD^{*\pm}X)/dp_t$ is shown in Fig. 10 for both analyses. Due to the different kinematic region of both analyses the cross sections can not be compared directly. The figure also includes the prediction of NLO QCD three flavour

massive calculations using the FMNR program and of the FONLL calculations. These calculations have large uncertainties due to the possible variations of the parameters. The central predictions of the FMNR program significantly underestimates the data in both kinematic regimes while FONLL is able to describe the tagged data but is below the untagged data especially at large p_t .

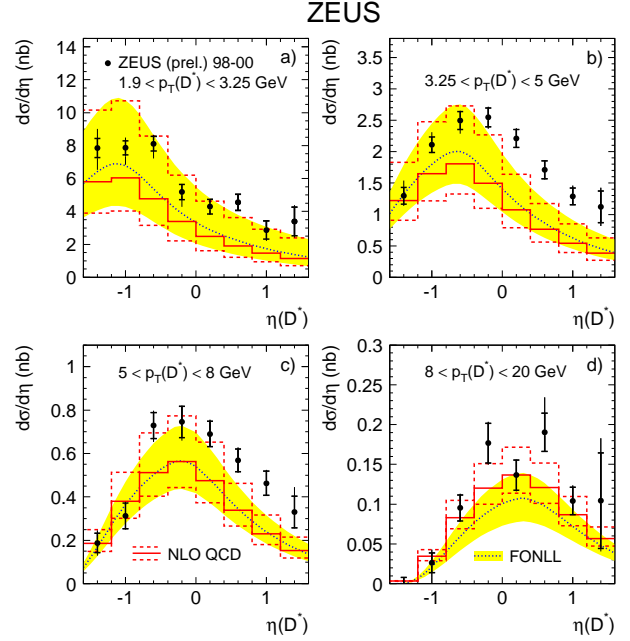


Fig.11: Differential cross sections $d\sigma(ep \rightarrow eD^{*\pm}X)/d\eta$ of the untagged data in four bins in p_t compared with predictions from NLO QCD and FONLL.

Due to the high statistics available at HERA also double differential cross sections are investigated. Fig.11 presents the cross section of the untagged γp data $d\sigma(ep \rightarrow eD^{*\pm}X)/d\eta$ in four bins in p_t . They are compared to the calculations of the NLO massive scheme and of FONLL as before. The discrepancy between theory and data becomes more evident in this double differential distributions. Both calculations fail to describe the data at medium p_t in the region $\eta > 0$. These data demonstrate well that the experimental precision obtained at HERA is capable to put significant constraints on theories.

5.1 Charm Di-jet Events in γp

The study of di-jet events in photoproduction of $D^{*\pm}$ meson has been proven to be an efficient tool for the investigation of the details of the charm production mechanism [32]. In terms of the LO picture a distinction between direct (Fig.1a) and resolved contributions (Fig.

1b-1d) becomes possible. From the reconstructed high energetic jets the momentum fraction of the photon contributing to the production of the two jets can be defined as

$$x_{\gamma}^{obs} = \frac{\sum_{jets} (E_T^{jet} e^{-\eta^{jet}})}{2yE_e}, \quad (2)$$

where yE_e is the initial photon energy and the sum is running over the two jets with the highest E_T^{jet} .

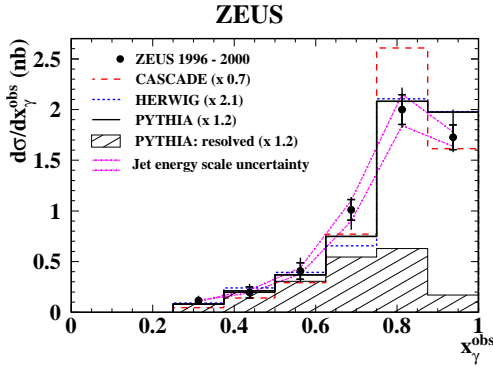


Fig. 12: Differential cross sections $d\sigma/dx_{\gamma}^{obs}$ compared with various MC simulations. See text for details.

Fig. 12 presents the differential cross section $d\sigma/dx_{obs}$ for the untagged sample [33]. The jets are reconstructed with the k_T cluster algorithm in its longitudinal invariant inclusive mode [29]. The events were required to have at least two jets with pseudo-rapidity $|\eta^{jet}| < 2.4$ and transverse energy $E_T^{jet} > 5$ GeV. The $D^{*\pm}$ mesons have been reconstructed in the visible range $|\eta^{D^*}| < 1.5$ and $p_T^{D^*} > 3$ GeV.

The peak in Fig. 12 at high values of x_{γ}^{obs} indicates a large direct photon contribution but there is also a sizable contribution from the resolved photon process at low x_{γ}^{obs} values. The data is compared with the predictions from the on-shell LO Monte Carlo simulations PYTHIA, HERWIG and the CCFM based CASCADE program. Since these programs predict total cross sections different from the measured one they are normalized to the data.

The best description of the shape is obtained by the PYTHIA program but also HERWIG is in good agreement with data. In order to describe the data with these programs a large resolved contribution of about 40% mainly due to $c^{(\gamma)}g^{(p)} \rightarrow cg$ (Fig. 1c,d) is required as indicated by the hatched area of Fig. 12.

The shape of the CASCADE prediction shows some deviations from the data at large values of x_{γ}^{obs} but is in good agreement at small x_{γ}^{obs} . It is worth mentioning that in this CCFM based calculation only the direct

process $\gamma g \rightarrow c\bar{c}$, depicted in Fig. 1a, contributes. The tail to small values of x_{γ}^{obs} is obviously a consequence of the off-shellness of the gluons in the calculation of the parton ladder emerging from the proton.

In order to understand better the mechanism of charm di-jet photoproduction in both, the resolved and the direct photon processes, the di-jet angular distribution has been investigated. This has been studied earlier for inclusive di-jet events [34]. In the jet-jet rest frame the differential cross section $d\sigma/d|\cos\Theta^*|$, where Θ^* is the angle between the proton beam direction and the jet axis, is sensitive to the spin of the propagator in the hard subprocess. In direct photon processes, where in the LO picture the propagator is a quark, the differential cross section is expected to be $d\sigma/d|\cos\Theta^*| \approx (1 - |\cos\Theta^*|)^{-1}$, while in resolved photon processes, where the propagator is most frequently a gluon, a steeper dependence on $|\cos\Theta^*|$, namely $d\sigma/d|\cos\Theta^*| \approx (1 - |\cos\Theta^*|)^{-2}$, should be observed.

As inferred from Fig. 12 in the LO picture most of the charm di-jet events from the resolved photon process are resulting from a large charm content in the photon, which is described by the diagrams of Fig. 1c and Fig. 1d. Although both diagrams contribute it turns out that the gluon exchange diagram Fig. 1d dominates. Consequently a large asymmetry is expected in the angular distribution $d\sigma/d\cos\Theta^*$ with respect to the charm jet direction, unambiguously defined by the $D^{*\pm}$ meson. The proton beam will lie more often in the hemisphere opposite to the charm jet direction. For the direct process of Fig. 1a, however, the $\cos\Theta^*$ distribution is expected to be symmetric with a smaller $|\cos\Theta^*|$ dependence because of the quark propagator.

The differential cross section $d\sigma/d\cos\Theta^*$ is compared in Fig. 13 with the normalized predictions of LO Monte Carlo programs PYTHIA and HERWIG separately for the resolved-enriched ($x_{\gamma}^{obs} < 0.75$) and the direct-enriched ($x_{\gamma}^{obs} > 0.75$) samples. As expected a large asymmetry of a strongly backward peaking cross section is observed in the resolved photon enriched sample supporting the LO interpretation of a large charm contribution to the photon structure. In the direct photon enhanced sample an almost symmetric $\cos\Theta^*$ distribution is observed with only very little $\cos\Theta^*$ dependence. The small enhancement in the backward hemisphere is due to contamination by the resolved process in this sample. The PYTHIA program reproduces well the shape of the distributions of both samples. The $\cos\Theta^*$ dependence is found to be less pronounced in the HERWIG calculation, especially the asymmetry in the

resolved-enriched sample is significantly smaller than observed in data.

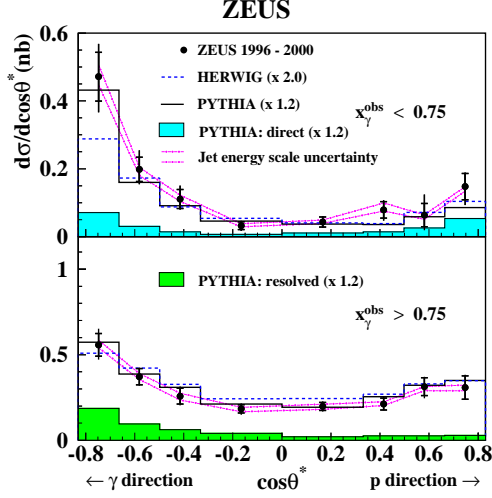


Fig.13: Differential cross sections $d\sigma/d\cos\Theta^*$ compared with MC simulations PYTHIA and HERWIG for the resolved-enriched ($x_\gamma^{obs} < 0.75$) and the direct-enriched ($x_\gamma^{obs} > 0.75$) samples. The model predictions are normalized to the data. See text for details.

In Fig. 14 the differential cross section $d\sigma/d\cos\Theta^*$ is compared with theoretical expectations. The results of the FMNR program are shown for two different ways of including jets in the calculation procedure. One procedure applies the k_T cluster algorithm to the partons. In the other approach these jets are subjected to hadronization corrections which are extracted from PYTHIA. In both cases the visibility cuts given above are applied to the resulting jets. Although the uncertainties due to the hadronization corrections are found to be quite large the pure parton level calculation agrees well with central values from the calculation with hadronization corrections. Both calculations agree well with the observed cross section $d\sigma/d\cos\Theta^*$ of the direct-enriched sample ($x_\gamma^{obs} > 0.75$) but systematically underestimate this cross section in the resolved-enriched regime ($x_\gamma^{obs} < 0.75$). However, due to the large hadronization uncertainties no strong conclusion can be made.

Fig. 14 also includes the absolute prediction of the CCFM evolution as implemented in CASCADE. This calculation significantly overshoots the data especially for ($x_\gamma^{obs} > 0.75$). However, when normalizing this calculation to the data the shape of the data is reasonably well described by CASCADE in both regimes. It should be stressed that currently the calculations in the CCFM evolution scheme are not complete. Neglecting the overall normalization problem CASCADE is in better agreement in shape with the

data than the massive NLO calculations. This may be interpreted as an indication for the important rôle of the parton's k_T in the parton evolution.

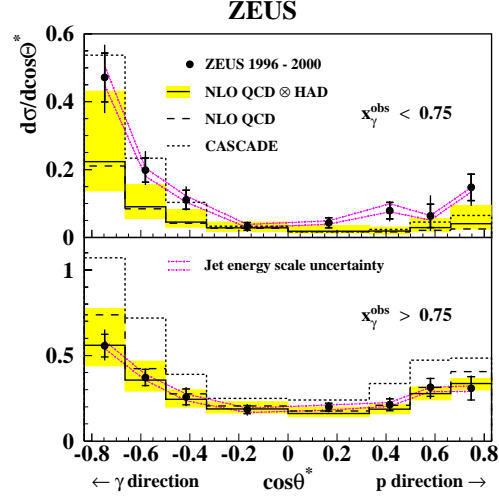


Fig.14: Differential cross sections $d\sigma/d\cos\Theta^*$ compared with the CASCADE and the massive NLO QCD predictions after hadronization correction and at the parton level for the resolved-enriched ($x_\gamma^{obs} < 0.75$) and the direct-enriched ($x_\gamma^{obs} > 0.75$) samples. See text for details.

6. Beauty Production

Although the cross section of beauty production is significantly smaller than that of charm production, it is of specific interest to investigate beauty production because QCD is considered to be more reliable due to the large scale m_b involved in the calculations.

The standard method of selecting a beauty enriched data sample is based on the semi-leptonic decays of b -hadrons. In the analyses presented here the observation of muons is used to tag beauty events. Since not only beauty hadrons but also charmed hadrons decay semi-leptonically the selection of muon events is not sufficient to obtain unambiguously beauty events. Another source for real muons is coming from the in-flight decays of pions and kaons. Finally, hadrons of which the hadronic showers are not completely absorbed in the calorimeters of the experiments may mimic muons. The two latter processes will be subsequently labeled as *fake muons*.

To get a separation between events with and without beauty additional features of b events and beauty hadrons have to be used. Because of the large value of m_b the invariant mass squared of the final state $b\bar{b}$ system, $\hat{s} = (P_b + P_{\bar{b}})^2$ has a high threshold of $4m_b^2 \approx 100 \text{ GeV}^2$. This allows for the enrichment of the muon event sample with b events

by additionally requiring the presence of at least one jet with high E_T^{jet} . Furthermore, also a consequence of the large mass m_b , the decay products from b -hadrons are expected to have relatively large opening angles with respect to the original b -hadron direction. Since

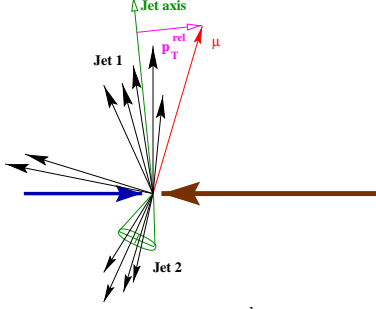


Fig.15: Sketch of the p_t^{rel} method for beauty tagging.

b -hadrons are not reconstructed the jet direction is taken instead. As sketched in Fig. 15 the muons from semi-leptonic b -hadron decay should have a relatively large angle or, equivalently, relatively large p_t^{rel} with respect to the jet axis. Due to the smallness of m_c compared to m_b the muons from semi-leptonic decay of charmed hadrons are expected to have small p_t^{rel} values. Fake muons are predominantly induced by hadrons from fragmentation. Because of the relatively small $\langle p_t \rangle$ in fragmentation they also should mainly contribute in the small p_t^{rel} region.

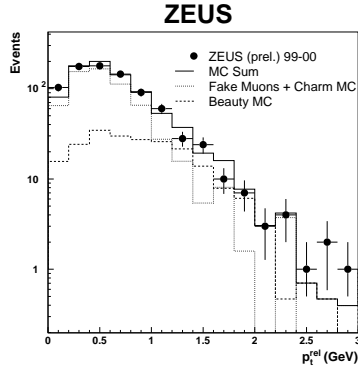


Fig.16: Observed p_t^{rel} distribution of muons in comparison to a MC fit to the data which includes contributions from fake muons plus charm MC and from beauty MC (shaded area).

In Fig. 16 the observed p_t^{rel} distribution for DIS events is plotted [35]. The events are selected in the kinematic region $Q^2 > 2 \text{ GeV}^2$ and $0.05 < y < 0.7$. The muon is restricted to the region of polar angle $30^\circ < \Theta_\mu < 160^\circ$ and momentum $p_\mu > 2 \text{ GeV}$. At least one jet has to be reconstructed in the Breit frame with the k_t cluster algorithm having an $E_{T,Breit}^{jet} > 6 \text{ GeV}$ and lying within the detector acceptance of $-2 < \eta_{lab}^{jet} < 2.5$ in the

laboratory frame. The distribution peaks at small values of p_t^{rel} where fake muons and muons from charmed hadron decays dominate. At large p_t^{rel} , however, the spectrum is harder than expected from light flavour and charm contributions only which indicates the presence of a sizable beauty contribution. To determine the amount of beauty events this distribution has been fitted by an arbitrary mixture of events from a light-plus-charm flavour and a beauty Monte Carlo program. The beauty fraction is $f_b = 0.25 \pm 0.05$. The sum of both Monte Carlo distribution reproduces the data well.

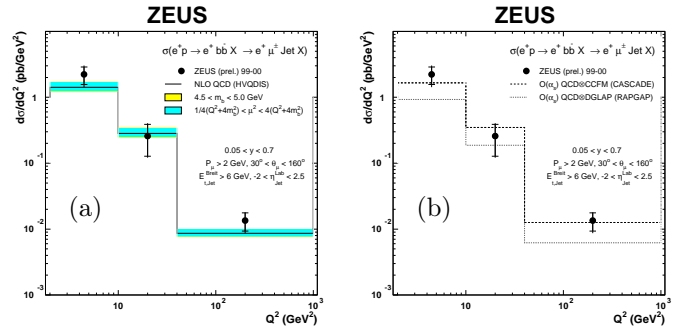


Fig.17: Differential cross section $d\sigma(ep \rightarrow ebb\bar{X} \rightarrow e\mu^\pm \text{Jet}X)/dQ^2$ in DIS in comparison with the expectation from (a) NLO QCD (HVQDIS) and (b) CCFM+PS (CASCADE) and LO+PS MC (RAPGAP). See text for details.

In Fig. 17 the differential cross section $d\sigma(ep \rightarrow ebb\bar{X} \rightarrow e\mu^\pm \text{Jet}X)/dQ^2$ in the visible range of the muon and the jet is presented in comparison with the expectation from the massive NLO calculation based on HVQDIS. For the fragmentation of the b quark into hadrons the Peterson function [7] with $\epsilon = 0.002$ has been used. The subsequent semi-leptonic decay was modeled using a parameterization of the muon momentum spectrum extracted from RAPGAP. The uncertainties due to the variation of the renormalization and factorization scale μ (inner shaded band) and of m_b (outer shaded band, when adding in quadrature) are also indicated. The data is somewhat above but agrees with the NLO predictions within the errors.

The predictions from the CCFM based CASCADE program and the LO RAPGAP simulation are also included in Fig.17. In both programs parton showers are included. While RAPGAP underestimates the visible beauty production cross section CASCADE is in good agreement with the data.

A similar analysis has been performed in photoproduction regime using the untagged sample [36]. here, the kinematic region is restricted to $Q^2 < 1 \text{ GeV}^2$ and $0.2 < y < 0.8$. The muons are selected by requiring

$-1.6 < \eta_\mu < 2.3$ and η_μ -dependent cuts on p_μ or $p_{t,\mu}$, respectively. Finally only those events are selected in which at least two jets with $p_T^{jet1(2)} > 7(6)$ GeV and $|\eta^{jet1,2}| < 2.5$ are reconstructed in addition.

Fig. 18 shows the differential cross section $d\sigma(ep \rightarrow b\bar{b} \rightarrow e\mu JJX)/dp_{t,\mu}$ in the visible range of the muon $-1.6 < \eta_\mu < 2.3$ and $p_{t,\mu} > 2.5$ GeV. The data is compared with the FMNR predictions without and with hadronization corrections taken from LO+PS Monte Carlo programs. The uncertainties due to the hadronization corrections are quite large. The central values of these calculations are a factor 1.4 below the data, but are still in reasonable agreement with the data when accounting for the errors and theoretical uncertainties.

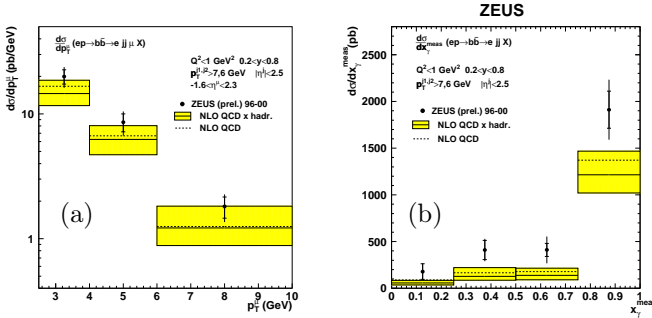


Fig.19: Differential beauty production cross sections (a) $d\sigma(ep \rightarrow b\bar{b} \rightarrow e\mu^\pm jjX)/dp_t$ and (b) $d\sigma(ep \rightarrow b\bar{b} \rightarrow ejjX)/dx_\gamma^{obs}$ compared with the massive NLO QCD calculations (FMNR). See text for details.

Since this analysis is based on the observation of at least two hard jets in the final state the momentum fraction of the photon x_γ^{obs} can be determined according to Eqn. 2. The differential beauty production cross section $d\sigma/dx_\gamma^{obs}$ is also shown in Fig. 18 in comparison with the prediction from the FMNR program. An experimental resolution of $x_\gamma \approx 0.2$ for this analysis has been estimated by Monte Carlo studies. Therefore, also the beauty production data indicates a large resolved photon contribution. The theoretical predictions, including the uncertainties due to hadronization effects, are significantly below the data. To extract this cross section experimentally large extrapolations beyond the visible range are necessary. These extrapolations are performed with help of LO Monte Carlo simulations. Differences between LO and NLO in the invisible part of phase space may be responsible for the larger disagreement.

To summarize the situation of beauty production at HERA it is interesting to note that the disagreement between data and theory tends to be smaller when

comparing beauty production cross sections in the phase space region directly accessible to the experiment compared to the case when large extrapolation factors are involved.

7. Conclusions

Recent results from HERA on open charm and beauty production in the γp and DIS regime have been presented. The high statistics available from the HERA-I running period allowed for detailed investigation of almost all theoretical questions related to heavy flavour production.

The measured fragmentation function and ratios at HERA are in good agreement with the results observed in other heavy quark production processes. With the reservation that there are some differences in extracting the information in the different fields, it has been shown that the QCD vacuum seen by the charm quark is independent from its production mechanism. This finding strongly supports the hypothesis of the universality of the charm quark fragmentation.

The detailed studies of single and double differential cross sections of inclusive $D^{*\pm}$ meson production have revealed sizable differences between data and theoretical calculations. The effect of using different evolution schemes in the theoretical calculations has been addressed. The predictions of the massive NLO DGLAP calculation using HVQDIS and of the CCFM evolution as implemented in CASCADE have been confronted with data. In DIS a better agreement of CASCADE with the measurement was observed in the inclusive $D^{*\pm}$ meson production cross sections. However, when requiring two jets to be visible in addition to the $D^{*\pm}$ meson all calculations and models failed to describe all aspects of the data simultaneously. Similar conclusions have been drawn from the investigations of $D^{*\pm}$ meson photoproduction. The data have been compared with calculations in the massive and massless NLO QCD and in the FONLL scheme. Although the theoretical uncertainties are large none of the calculations was able to describe the data within the theoretical parameter space currently considered.

The analysis of $D^{*\pm}$ mesons with associated di-jet production in the γp regime have confirmed the presence of a large charm content in the photon in the LO picture of photoproduction. The data could be also interpreted to show that the parton's k_t plays an important rôle in the parton ladder emerging from the proton. A charm double tag analysis could resolve this ambiguity.

Finally results on differential beauty production

cross section in γp and DIS have been presented. Within the experimental errors and the large theoretical uncertainties coming from hadronization effects no strong statement on the agreement between data and theory can be made if cross sections in the experimentally accessible range are considered. If, however, cross sections in full phase space are considered large discrepancies between data and theory are observed. This problem may be due to the absence of NLO Monte Carlo programs to perform the extrapolation from the visible range to full phase space in a way consistent with theory.

In general the current precision of the heavy flavour production data at HERA is superior to the uncertainties in the theoretical calculations. Therefore these data can be used to constrain significantly the theory. In order to use the full potential of the heavy flavour data from HERA more theoretical efforts are needed to reduce the theoretical uncertainties and to give a better description of all observations.

1. E. Laenen *et al.*, *Nucl. Phys.***B 392** 162,229 (1993), *Nucl. Phys.***B 291** 325 (1992); S. Riemersma, J. Smith, and W.L. van Neerven: *Phys. Lett.* **B 347** 142 (1995).
2. S. Frixione *et al.*, *Phys. Lett.* **B 348** 633 (1995).
3. B.W. Harris and J. Smith, *Nucl. Phys.* **B 452** 109 (1995), *Phys. Lett.* **B 353** 535 (1995).
4. R.K. Ellis and P. Nason, *Nucl. Phys.* **B 312** 551 (1989); P. Nason, S. Dawson and R.K. Ellis, *Nucl. Phys.* **B 303** 607 (1988), *Nucl. Phys.* **B 327** 49 (1989).
5. B.W. Harris and J. Smith, *Phys. Rev.* **D 57** 2806 (1998).
6. M.L. Mangano, P. Nason and G. Ridolfi, *Nucl. Phys.* **B 373** 295 (1992); S. Frixione *et al.* *Nucl. Phys.* **B 412** 225 (1994).
7. C. Peterson *et al.*, *Phys. Rev.* **D 27** 105 (1983).
8. B.A. Kniehl *et al.*, *Z. Phys.* **C 76** 689 (1997); M. Cacciari and M. Greco, *Phys. Rev.* **D 55** 7134 (1997); J. Binnewies *et al.*, *Z. Phys.* **C 76** 677 (1997).
9. J. Binnewies *et al.*, *Phys. Rev.* **D 58** 014014 (1998).
10. M.A.G. Aivasis *et al.*, *Phys. Rev.* **D 50** 3102 (1994).
11. M. Cacciari, S. Frixione and P. Nason, [[hep-ph/0102134](#)].
12. M. Ciafaloni, *Nucl. Phys.* **B 296** 49 (1988); S. Catani, F. Fiorani and G. Marchesini, *Phys. Lett.* **B 234** 339 (1990), *Nucl. Phys.* **B 336** 18 (1990); G. Marchesini, *Nucl. Phys.* **B 445** 45 (1995).
13. H. Jung, Proc. 7th DIS Workshop, *Nucl. Phys.* **B 79** 429 (1999) (Proc. Suppl.), [[hep-ph/9905554](#)].
14. H. Jung, Proc. Workshop on Monte Carlo Generators for HERA Physics, 1999, DESY-PROC-1999-02, p.75, [[hep-ph/9908497](#)]; H. Jung and G. Salam, to be published.
15. S.P. Baranov, H. Jung and N.P. Zotov, Proc. Workshop on Monte Carlo Generators for HERA Physics, 1999, DESY-PROC-1999-02, p.484.
16. S. Aid *et al.* (H1 Collab.), *Nucl. Phys.* **B 470** 3 (1996).
17. ZEUS Collab. contributed paper to the *International Europhysics Conference on High Energy Physics*, Aachen, **Abstract # 564** (2003).
18. H1 Collab., contributed paper to the *International Europhysics Conference on High Energy Physics*, Aachen, **Abstract # 096** (2003).
19. F. Becattini, *Z. Phys.* **C69** 485 (1996).
20. Yi-Jin Pei, *Z. Phys.* **C72** 39 (1996).
21. L. Gladilin, Preprint [[hep-ex/9912064](#)], (1999).
22. ZEUS Collab., contributed paper to the *XXXIst International Conference on High Energy Physics*, Amsterdam, **Abstract # 778** (2002).
23. H. Albrecht *et al.*, (ARGUS Collab.), *Z. Phys.* **C53** 353 (1991).
24. R. Akers *et al.*, (OPAL Collab.) *Z. Phys.* **C67** 27 (1995).
25. H1 Collab., contributed paper to the *International Europhysics Conference on High Energy Physics*, Aachen, **Abstract # 098** (2003).
26. H.L. Lai *et al.*, *Eur. Phys. J* **C 12** 375 (2000).
27. R. Barate *et al.*, (ALEPH Coll.) *Eur. Phys. J* **C 16** 597 (2000) [[hep-ex/9909032](#)].
28. H. Jung, *Comp. Phys. Comm.* **86** 147 (1995).
29. S. Catani *et al.*, *Nucl. Phys.***B 406** 187 (1993); S.D. Ellis and D.E. Soper, *Phys. Rev.* **D 48** 3160 (1993).
30. ZEUS Collab., contributed paper to the *XXXIst International Conference on High Energy Physics*, Amsterdam, **Abstract # 786** (2002).
31. H1 Collab., contributed paper to the *International Europhysics Conference on High Energy Physics*, Aachen, **Abstract # 097** (2003).
32. J. Breitweg *et al.*, *Eur. Phys. J.* **C 6** 67 (1999).
33. S. Chekanov *et al.* (ZEUS Collab.), accepted by *Phys. Lett* **B** (2003), [[hep-ex/0302025](#)].
34. M. Derrick *et al.* (ZEUS Collab.), *Phys. Lett* **B 384** 401 (1995); S. Chekanov *et al.* (ZEUS Collab.), *Eur. Phys. J.* **C 23** 615 (2002).
35. ZEUS Collab., contributed paper to the *XXXIst International Conference on High Energy Physics*, Amsterdam, **Abstract # 782** (2002).
36. ZEUS Collab., contributed paper to the *XXXIst International Conference on High Energy Physics*, Amsterdam, **Abstract # 785** (2002).